

Binding distance of  $c(2 \times 2)$  O on Ni(001)

S. Y. Tong and K. H. Lau\*

*Department of Physics and Surface Studies Laboratory, University of Wisconsin-Milwaukee, Milwaukee, Wisconsin 53201*

(Received 4 February 1982)

The binding distance of  $c(2 \times 2)$  O on Ni(001) was studied in detail by low-energy electron diffraction. We calculated intensity-voltage curves at normal and off-normal incidences for O-Ni interlayer spacings 1.3 Å down to 0.0 Å, using the combined-space method. Comparisons with experimental data show that there is no improved agreement for any of the spacings over the original value of  $d_{\perp} = 0.9$  Å. However, the values of  $d_{\perp} = 0.9$  and  $d_{\perp} \leq 0.1$  Å show roughly the same fit. A normalized  $R$  factor also gives double minima of approximately the same depth at these two spacings.

## I. INTRODUCTION

The binding distances of chalcogens (Te, Se, S, and O) adsorbed on Ni(001) are probably the most studied structural parameters in recent surface crystallography. It was known from early low-energy electron diffraction (LEED) experiments<sup>1-3</sup> that two ordered structures can be obtained: a  $p(2 \times 2)$  pattern which appears at coverage  $\theta < 0.25$  and a  $c(2 \times 2)$  pattern at  $\theta < 0.5$ . The first structural determination of chalcogens on Ni(001) was done by LEED: It was determined that on Ni(001), the  $p(2 \times 2)$  and  $c(2 \times 2)$  chalcogens all bind at the hollow site.<sup>4,5</sup> The LEED studies also determined the perpendicular spacing  $d_{\perp}$  between the chalcogen layer and the top Ni layer. For  $p(2 \times 2)$  and  $c(2 \times 2)$  overlayers of Te, Se, and S, the LEED-determined  $d_{\perp}$  spacings are well corroborated by subsequent determinations using other spectroscopic techniques and by results of *ab initio* calculations.

The binding distance of O on Ni(001) is, however, less certain. While the value of  $d_{\perp}$  for the  $p(2 \times 2)$  coverage, determined by LEED to be 0.9 Å above Ni(001),<sup>5</sup> remains unchallenged, the value of  $d_{\perp}$  for the  $c(2 \times 2)$  coverage varied among analyses. From the very beginning, early LEED studies produced conflicting results. Andersson *et al.*<sup>6</sup> and Demuth *et al.*<sup>4</sup> reported  $d_{\perp}$  values of 1.5 and 0.9 Å, respectively. Duke *et al.*<sup>7</sup> concluded that the oxygen atoms replaced half of the Ni atoms at the surface, thus forming a Ni-O square lattice with a  $c(2 \times 2)$  periodicity, which sits on the Ni(001) substrate. Later analysis by LEED using more extensive data supported the 0.9-Å distance of Demuth *et al.*<sup>8,9</sup>

Recently, rapid LEED intensity measurements by Hanke *et al.*<sup>10</sup> and ion scattering spectroscopy (ISS) by Brongersma and Theeten<sup>11</sup> showed that  $d_{\perp} = 0.9$  Å. Results of photoelectron diffraction (PD) by Rosenblatt *et al.*<sup>12</sup> are consistent with a  $d_{\perp} = 0.9$  Å, although no analysis was done for  $d_{\perp} < 0.5$  Å. Brundle and Hopster<sup>13</sup> saw no difference in character in the x-ray photoemission spectroscopy (XPS) data of  $p(2 \times 2)$  and  $c(2 \times 2)$  coverages; therefore, they concluded that the ordered structures are at  $d_{\perp} = 0.9$  Å for both coverages. These authors, on the other hand, did see a large change in the XPS character between either  $c(2 \times 2)$  or  $p(2 \times 2)$  overlayer and a NiO double-layer nucleation.

Other studies have yielded quite different conclusions. Azimuthal photoelectron diffraction (APD) by Petersson *et al.*<sup>14</sup> found that at low coverage,  $d_{\perp} = 0.9$  Å, but at sufficiently high coverages, the oxygen moved down to be nearly coplanar with the nickel:  $d_{\perp} \approx 0.0$  Å. High-resolution electron-energy-loss spectroscopy (EELS) data by Andersson<sup>15,16</sup> and by Lehwald and Ibach<sup>17</sup> show that the oxygen-derived vibration frequencies are qualitatively different between  $p(2 \times 2)$  and  $c(2 \times 2)$  coverages. The data by Andersson<sup>15,16</sup> and by Dalmi-Imelik *et al.*<sup>18</sup> also show that the oxygen-derived vibration-loss frequencies for the simple overlayers [i.e.,  $p(2 \times 2)$  and  $c(2 \times 2)$ ] are very different (much lower) than those from nickel-oxide films or intermediate-oxide states on the nickel surface. A recent lattice-dynamical calculation by Rahman *et al.*<sup>19</sup> using the potential-energy curve produced in Upton and Goddard's<sup>20</sup> calculation fitted the  $p(2 \times 2)$  EELS data with  $d_{\perp} = 0.88$  Å and the  $c(2 \times 2)$  data with  $d = 0.27$  Å.

In view of these conflicting results and the fact that the previous LEED calculations were not done for  $d < 0.6$  Å, we carried out a new LEED analysis for  $c(2 \times 2)$  O-Ni(001) with  $d_1 = 1.3$  Å and varied the spacing down to 0.0 Å. Our aim is to determine whether or not the LEED intensity-voltage (IV) data can definitively rule out the small- $d_1$  result. The reason previous LEED calculations stopped at  $d_1 = 0.6$  Å was that the Bloch waves between atomic layers were expanded in terms of  $g$  plane waves. The number  $g$  increases rapidly as  $d_1^{-2}$ . For  $d_1 < 0.6$  Å, the dimension of the scattering matrices becomes very large.

This difficulty is avoided by the use of the combined-space method,<sup>21</sup> which accurately handles layers with any separation distance. In this work, we compare the calculations of IV curves at normal and off-normal incidences using 10 values of  $d_1$  and compare our calculated results with the data of Demuth and Rhodin.<sup>22</sup> In Sec. II, we present details of the calculation and its inputs. Section III presents the comparison between theory and experiment of IV curves and results of an averaged  $R$  factor. Our conclusions are given in Sec. IV.

## II. METHOD OF COMPUTATION AND INPUT PARAMETERS

To calculate LEED intensity energy (IV) spectra for general adsorbate-substrate  $d_1$  spacings, we used the combined-space method of Tong and Van Hove.<sup>21</sup> In this method, the oxygen overlayer and the topmost nickel layer are treated as a composite layer in which the layer scattering matrices are solved in  $L$  (angular momentum) space. These matrices are then transformed to the  $K$ - (linear momentum) space representation. Multiple scatterings between the composite layer and the other (nickel) layers are solved in  $K$  space. Since the method does not use  $K$ -space expansions within the composite layer, it avoids the use of too many beams when  $d_1$  gets small between atomic layers of the composite.

For inputs to the LEED computer program, the nickel phase shifts are calculated from the self-consistent band-structure potential of Wakoh,<sup>23</sup> and oxygen phase shifts are obtained from a self-consistent  $X\alpha$  scattered-wave calculation of a  $Ni_5O$  cluster. The imaginary part of the optical potential is given by

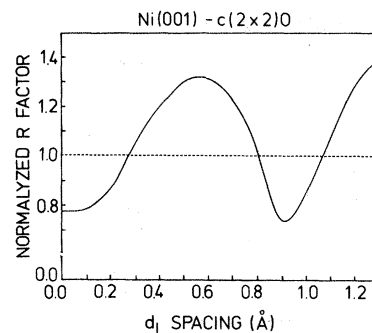


FIG. 1. The normalized  $R$  factor vs  $d_1$  spacing between O layer and nickel (001) surface.

$$V_I = 3.8 \left[ \frac{E + V_0}{90 + V_0} \right]^{1/3},$$

where  $V_I$  is measured in units of eV,  $E$  is the energy in electron volts above vacuum, and  $V_0$  is the inner potential. Although we initially used  $V_0 = 11.2$  eV,<sup>24</sup> our  $R$ -factor analysis preferred a value of  $V_0 = 13.2$  eV. All the figures shown in Sec. III are with  $V_0 = 13.2$  eV. The 2-eV shift slightly improved our normalized  $R$  factor but has little effect on the conclusions of the  $d$  spacing.

## III. COMPARISON OF IV CURVES BETWEEN THEORY AND EXPERIMENT AND RESULTS OF THE AVERAGED $R$ FACTOR

Calculations of IV curves in the energy range 20–240 eV are made. Ten  $d_1$  spacings, ranging

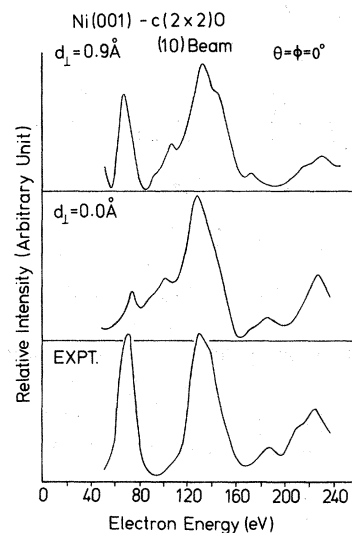


FIG. 2. Comparison between theory and experiment: (10) beam at normal incidence.

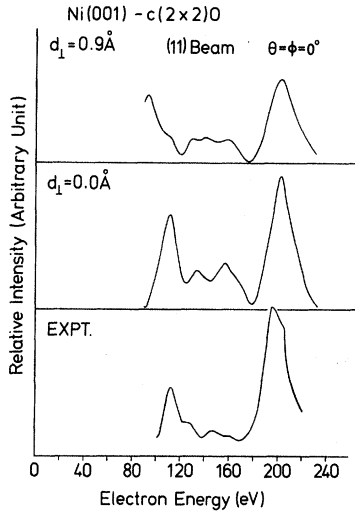


FIG. 3. Comparison between theory and experiment: (11) beam at normal incidence.

from  $d_1=0.0$  to  $1.3 \text{ \AA}$  are chosen. Comparisons are made with the experimental data of Demuth and Rhodin<sup>22</sup> at normal incidence for the (10), (11), and  $(\frac{1}{2} \frac{1}{2})$  beams and at  $\theta=4^\circ, 8^\circ, 14^\circ,$  and  $20^\circ$  for the (00) beam. To facilitate comparison with the experimental data, we use six  $R$  factors defined earlier by Van Hove *et al.*,<sup>25</sup> Zanazzi and Jona,<sup>26</sup> and Pendry,<sup>27</sup> and construct a normalized  $R$  factor. First, we put weights on the individual  $R$  factors, defined as follows:

$$R_1 = A_1 \Delta E_s / \Delta E_{\text{tot}}, \quad (1)$$

$$R_2 = A_2 \int (I_e - cI_t)^2 dE, \quad (2)$$

$$R_3 = A_3 \int (I'_e - cI'_t)^2 dE, \quad (3)$$

$$R_4 = A_4 \int (I''_e - cI''_t)^2 dE, \quad (4)$$

$$R_5 = A_5 \int \frac{|I'_e - cI'_t| |I''_e - cI''_t|}{|I'_e| + \max |I'_e|} dE, \quad (5)$$

$$R_6 = A_6 \frac{\int (Y_e - Y_t)^2 dE}{\int (Y_e^2 + Y_t^2) dE}, \quad (6)$$

where  $\Delta E_s$  is the energy range with slopes of opposite signs,  $\Delta E_{\text{tot}}$  is the total energy range,  $I_e$  is the experimental intensity data,  $I'_e$  and  $I''_e$  refer to the first and second derivatives of  $I_e$  with respect to energy;  $I_t, I'_t,$  and  $I''_t$  are the corresponding quantities for the calculated intensities. Also,

$$C = \frac{\int I_e dE}{\int I_t dE} \quad (7)$$

and

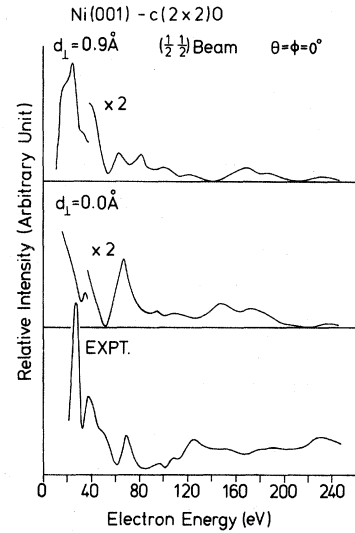


FIG. 4. Comparison between theory and experiment:  $(\frac{1}{2} \frac{1}{2})$  beam at normal incidence.

$$Y_{e,t} = \frac{I'_{e,t}/I_{e,t}}{1 + V_I^2 \left[ \frac{I'_{e,t}}{I_{e,t}} \right]^2}. \quad (8)$$

The weights  $A_1, \dots, A_6$  are chosen such that the average value of each  $R$  factor over the geometries considered in this work is 1.0. This ensures that the influence of each  $R$  factor is roughly the same, and in taking the overall average, no one  $R$  factor dominates the others. We then define our normalized  $R$  factor as the mean of  $R_1, \dots, R_6$ , each having been weighted by the coefficients  $A_1, \dots, A_6$ .

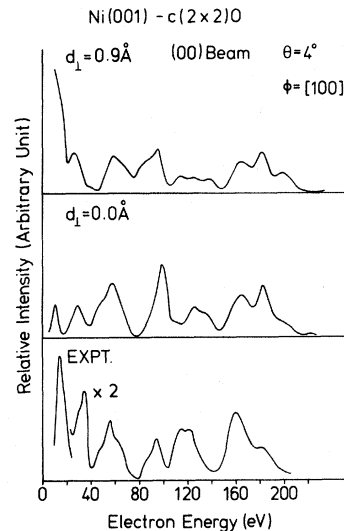


FIG. 5. Comparison between theory and experiment: (00) beam at  $\theta=4^\circ$ ,  $\phi$  along [100] direction.

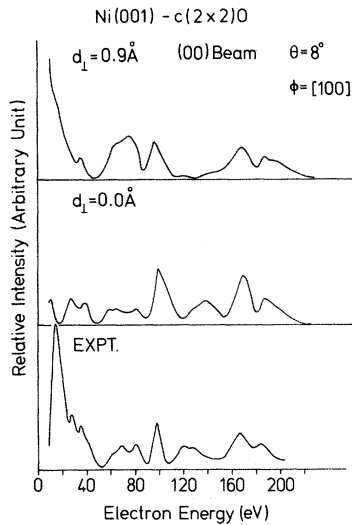


FIG. 6. Comparison between theory and experiment: (00) beam at  $\theta=8^\circ$ ,  $\phi$  along [100] direction.

The normalized  $R$  factor, based on the seven IV curves [the (10), (11), ( $\frac{1}{2} \frac{1}{2}$ ) beams at normal incidence and the (00) beam at  $\theta=4^\circ, 8^\circ, 14^\circ$ , and  $20^\circ$ ], plotted as a function of  $d_\perp$ , shows two roughly equal minima, at  $d_\perp \leq 0.1 \text{ \AA}$  and  $d_\perp = 0.9 \text{ \AA}$  (Fig. 1). A pronounced peak occurs between them at  $d_\perp \approx 5.5 \text{ \AA}$ . The  $R$ -factor value changes by more than 78% between either minima and this peak. Of the two minima, the  $R$  factor at  $d_\perp = 0.9 \text{ \AA}$  is 6% lower. Thus, the agreement between theory and experiment at "best" fit is at  $d_\perp = 0.9 \text{ \AA}$ . The agreement deteriorates at  $d_\perp \approx 5-6 \text{ \AA}$  but then improves again as  $d_\perp$  nears zero.

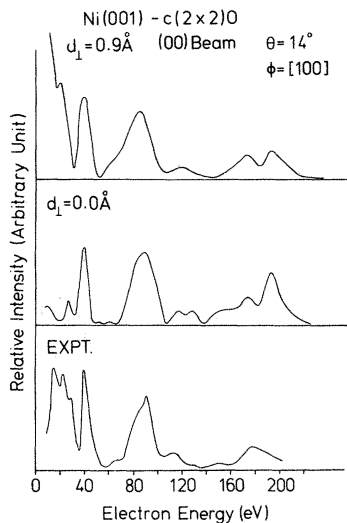


FIG. 7. Comparison between theory and experiment: (00) beam at  $\theta=14^\circ$ ,  $\phi$  along [100] direction.

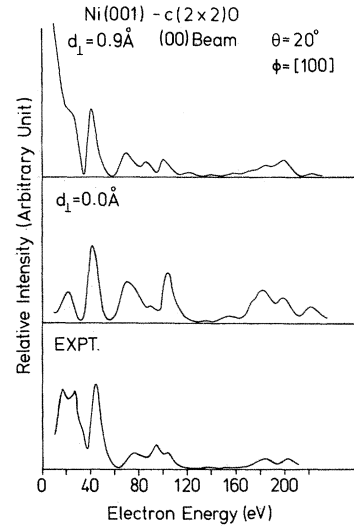


FIG. 8. Comparison between theory and experiment: (00) beam at  $\theta=20^\circ$ ,  $\phi$  along [100] direction.

The overall agreement between theory and experiment is acceptable, but not outstanding, even at  $d_\perp = 0.9 \text{ \AA}$ . We can see this from the value of the Zanazzi-Jones (ZJ)  $R$  factor,<sup>26</sup> which is 0.27 at  $d_\perp = 0.9 \text{ \AA}$  and 0.29 at  $d_\perp = 0.0 \text{ \AA}$ . We normally classify a good fit if  $R_{ZJ} < 0.2$ . The agreement, however, is better at normal incidence:  $R_{ZJ} = 0.14$  at  $d_\perp = 0.9 \text{ \AA}$  and  $R_{ZJ} = 0.16$  at  $0.0 \text{ \AA}$  if we count only the comparison at normal incidence.

The calculated IV curves, together with the experimental data, are shown for the two best  $d$  spacings in Figs. 2–8. Of the seven IV curves, only the ( $\frac{1}{2} \frac{1}{2}$ ) beam is an overlayer (oxygen) spot. The

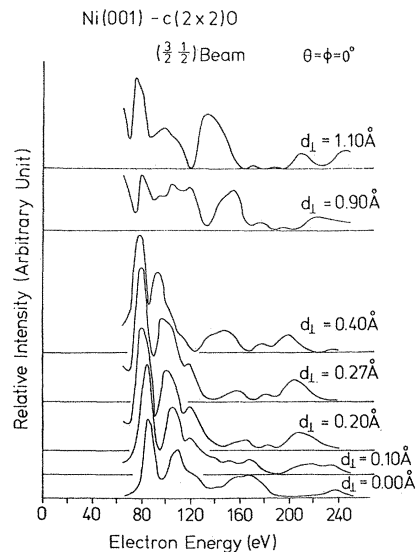


FIG. 9. Calculated IV curves for the ( $\frac{3}{2} \frac{1}{2}$ ) beam at normal incidence, showing several  $d_\perp$  spacings.

others are all substrate spots. An IV curve from a substrate spot is not very sensitive to the oxygen-nickel spacing because many of the peaks in the curve are derived from scatterings between nickel layers, which are independent of the O-Ni spacing.

We show in Fig. 9 another overlayer spot: the  $(\frac{3}{2} \frac{1}{2})$  beam. This beam does not appear until  $E \geq 80$  eV, however, it does contain a few peaks. Its intensity at 82 eV is about 40% of the experimental peak in the  $(\frac{1}{2} \frac{1}{2})$  beam at 70 eV. This beam is very different between  $d_{\perp} = 0.0$  Å and  $d_{\perp} = 0.9$  Å. It seems that further analysis by LEED should concentrate on the  $(\frac{1}{2} \frac{1}{2})$  and  $(\frac{3}{2} \frac{1}{2})$  beams. The problem, of course, is that these two beams have little intensity at  $E \geq 60$  eV at room temperature. Perhaps low-temperature IV curves should be taken.

#### IV. CONCLUSIONS

Our analysis indicates that when comparing calculated LEED IV curves with the data of Demuth and Rhodin,<sup>22</sup> the  $d_{\perp} = 0.9$  Å is slightly favored. However, by extending the comparison of  $d_{\perp}$  to include  $d_{\perp} = 0.0$  Å, we found that the LEED analysis cannot rule out the structure that has oxygen atoms close ( $d_{\perp} \approx 0.0$  Å) to the Ni(001) surface. Based on the calculated IV curves for the oxygen-derived beams [(i.e.,  $(\frac{1}{2} \frac{1}{2})$  and  $(\frac{3}{2} \frac{1}{2})$ ], it is clear that if these beams can be measured experimental-

ly, they could be used to better differentiate between the two  $d_{\perp}$  spacings. We suggest that low-temperature IV curves be taken.

On the other hand, the evidence from EELS is rather striking. It indicates that there is an oxygen  $c(2 \times 2)$  phase which is *qualitatively* different from the  $p(2 \times 2)$  or nickel-oxide phases. The question is, at what oxygen coverage does the EELS loss peak at  $430 \text{ cm}^{-1}$  shift down to  $310 \text{ cm}^{-1}$ ? Does this "down shift" coincide exactly with the disappearance of the  $p(2 \times 2)$  LEED spots? Rosenblatt *et al.*<sup>12</sup> stated that their photoelectron diffraction data were taken at an oxygen coverage where the last evidence of  $p(2 \times 2)$  spots disappeared and the  $c(2 \times 2)$  pattern became sharp. Does this occur at the same oxygen coverage where EELS observed the down-shifted loss peak of  $310 \text{ cm}^{-1}$ ? Experimental clarification of these points will help to better define the  $c(2 \times 2)$  phase or phases of oxygen on Ni(001).

#### ACKNOWLEDGMENTS

We acknowledge informative discussions on the subject matter with Dr. J. E. Demuth, Dr. P. M. Marcus, Dr. D. L. Mills, Dr. C. R. Brundle, and Dr. D. H. Rosenblatt. This work was supported by NSF Grant No. DMR8101203, the Petroleum Research Fund, Grant No. 11584-AC5,6, and DOE Grant No. DE-AC02-79ER10431.

\*Present address: Bell Laboratories, Murray Hill, N. J. 07974

<sup>1</sup>H. E. Farnsworth and H. H. Madden, Jr., *J. Appl. Phys.* **32**, 1933 (1961).

<sup>2</sup>R. L. Park and H. E. Farnsworth, *J. Chem. Phys.* **43**, 2351 (1965).

<sup>3</sup>A. V. MacRae, *Surf. Sci.* **1**, 319 (1964).

<sup>4</sup>J. E. Demuth, D. W. Jepsen, and P. M. Marcus, *Phys. Rev. Lett.* **31**, 540 (1973).

<sup>5</sup>M. A. Van Hove and S. Y. Tong, *J. Vac. Sci. Technol.* **12**, 230 (1975).

<sup>6</sup>S. Andersson, B. Kasemo, J. B. Pendry, and M. A. Van Hove, *Phys. Rev. Lett.* **31**, 595 (1973).

<sup>7</sup>C. B. Duke, N. O. Lipan, and G. E. Laramore, *Nuovo Cimento* **23B**, 241 (1974).

<sup>8</sup>M. Scheffler, K. Kambe, F. Forstman, and K. Jacobi, in *Proceedings of the 7th International Vacuum Congress and 3rd International Conference on Solid Surfaces, Vienna, 1977*, edited by R. Dobrozemsky *et al.* (Berger and Söhne, Vienna, 1977), p. 2223.

<sup>9</sup>T. N. Rhodin and S. Y. Tong, *Physics Today* **28**, 10

(1975).

<sup>10</sup>G. Hanke, E. Lang, K. Heinz, and K. Müller, *Surf. Sci.* **91**, 551 (1980).

<sup>11</sup>H. H. Brongersma and J. B. Theeten, *Surf. Sci.* **54**, 519 (1976).

<sup>12</sup>D. H. Rosenblatt, J. G. Tobin, M. G. Mason, R. F. Davis, S. D. Kevan, D. A. Shirley, C. H. Li, and S. Y. Tong, *Phys. Rev. B* **23**, 3828 (1981).

<sup>13</sup>C. R. Brundle and H. Hopster, *J. Vac. Sci. Technol.* **18**, 663 (1981).

<sup>14</sup>L. G. Petersson, S. Kono, N. F. T. Hall, S. Goldberg, J. T. Lloyd, C. S. Fadley, and J. B. Pendry, *Mater. Sci. Eng.* **42**, 111 (1980).

<sup>15</sup>S. Andersson, *Solid State Commun.* **20**, 229 (1976).

<sup>16</sup>S. Andersson, *Surf. Sci.* **79**, 385 (1979).

<sup>17</sup>S. Lehwald and H. Ibach, in *Proceedings of the International Conference on Vibrations at Surfaces, Namur, Belgium, 1980*, edited by A. Lucas (Pergamon, New York, 1982).

<sup>18</sup>G. Dalmai-Imelik, J. C. Bertolini, and J. Rousseau, *Surf. Sci.* **63**, 67 (1977).

- <sup>19</sup>T. S. Rahman, J. E. Black, and D. L. Mills, Phys. Rev. Lett. 46, 1469 (1981).
- <sup>20</sup>T. H. Upton and W. A. Goddard III, Phys. Rev. Lett. 46, 1635 (1981).
- <sup>21</sup>S. Y. Tong and M. A. Van Hove, Phys. Rev. B 16, 1459 (1977).
- <sup>22</sup>J. E. Demuth and T. N. Rhodin, Surf. Sci. 45, 249 (1974).
- <sup>23</sup>S. Wakoh, J. Phys. Soc. Jpn. 20, 1894 (1965).
- <sup>24</sup>S. Y. Tong and L. L. Kesmodel, Phys. Rev. B 8, 3753 (1973).
- <sup>25</sup>M. A. Van Hove, S. Y. Tong, and M. H. Elconin, Surf. Sci. 64, 85 (1977).
- <sup>26</sup>E. Zanazzi and F. Jona, Surf. Sci. 62, 61 (1977).
- <sup>27</sup>J. B. Pendry, J. Phys. C 13, 937 (1980).